PHYSICAL REVIEW C, VOLUME 63, 031301(R)

Isoscalar giant dipole resonance in ^{90}Zr, ^{116}Sn, and ^{208}Pb

H. L. Clark, Y.-W. Lui, and D. H. Youngblood

Cyclotron Institute, Texas A&M University, College Station, Texas 77845

(Received 30 August 2000; published 31 January 2001)

Strength functions for isoscalar dipole excitations in ^{90}Zr, ^{116}Sn, and ^{208}Pb have been measured with inelastic scattering of 240 MeV α particles at small angles. The isoscalar $E1$ strength distribution in each nucleus is found to consist of a broad component at $E_x \sim 114/A^{1/3}$ MeV containing approximately 100% of the $E1$ EWSR and a narrower one at $E_x \sim 72/A^{1/3}$ MeV containing 15–28 % of the total isoscalar $E1$ strength. The higher component is the compression mode $E1$ strength previously reported only in ^{208}Pb, whereas the lower component may be a new mode not reported previously, but suggested by recent RPA-HF and relativistic mean field calculations.

DOI: 10.1103/PhysRevC.63.031301 PACS number(s): 25.55.Ci, 24.30.Cz, 27.60.+j, 27.80.+w

Evidence for a broad isoscalar giant dipole resonance (ISGDR) at $E_x \sim 21$ Mev in ^{208}Pb has been reported by several groups [1–4]. The structure, transition density and sum rule for this $3\hbar\omega$ resonance, a result of the operator $r^3 Y_{10}$, have been described by Deal [5], Harakeh [6], and Stringari [7]. It is of particular interest because it is a compression mode and like the isoscalar giant monopole resonance (GMR), its energy can be related to compressibility [7]. In the scaling model

$$E_1 = \hbar[7(K_A + 27/25^* \varepsilon_F)/3m\langle r^2 \rangle]^{1/2},$$

where K_A is the nuclear compressibility and ε_F is the Fermi energy. Van Giai and Sagawa [8] using the Skyrme interaction in Hartree-Fock (HF) random phase approximation (RPA) calculations found the $r^3 Y_{10}$ $E1$ strength at about $E_x \sim 25$ MeV in ^{208}Pb.

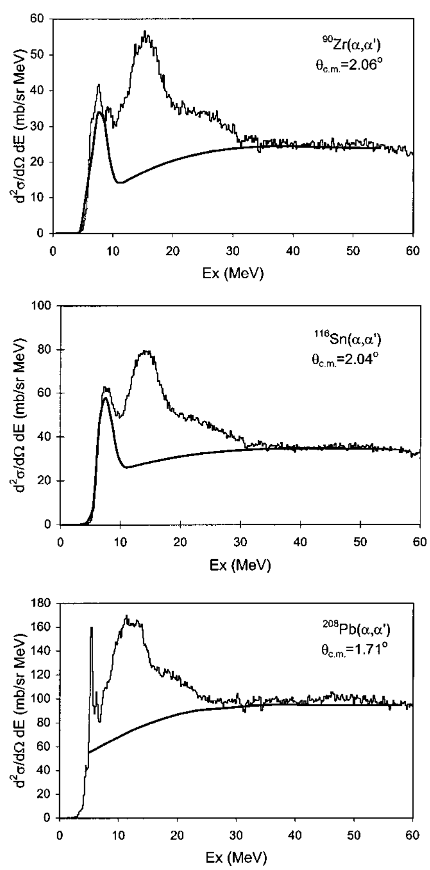

FIG. 1. Inelastic α spectra obtained near the peak of the ISGDR for ^{90}Zr, ^{116}Sn, and ^{208}Pb. The solid lines show the continuum chosen for the analysis and the LEOR contribution for ^{90}Zr and ^{116}Sn.

We have investigated the giant resonance regions in ^{90}Zr, ^{116}Sn, and ^{208}Pb using inelastic scattering of 240 MeV α particles where excellent peak to continuum ratios are obtained [9–11] and where competing pickup-breakup reactions are well above the region where ISGDR strength is expected. GMR strengths extracted from this data have already been reported [12]. The experimental technique has been described thoroughly in Refs. [9–12]. Sample spectra obtained are shown in Fig. 1. The prominent giant quadrupole resonance (GQR) and GMR are obvious as is a weaker and broader peak at higher excitation that moves systematically with mass.

The transition density for the ISGDR is [6]

$$\rho(r) = -\beta_1/R\sqrt{3}[3r^2 d/dr + 10r - 5/3\langle r^2 \rangle d/dr + \epsilon(r d^2/dr^2 + 4d/dr)]\rho_o(r).$$

For one state which exhausts the energy weighted sum rule [6]

$$\beta_1{}^2 = (6\pi\hbar^2/mAE_x)R^2/(11\langle r^4 \rangle - 25/3\langle r^2 \rangle^2 - 10\epsilon\langle r^2 \rangle),$$

where $\epsilon = (4/E_2 + 5/E_0)\hbar^2/3mA$ and E_2 and E_0 are quadrupole and monopole giant resonance energies, respectively. In these nuclei the isovector giant dipole resonance (IVGDR) is

TABLE I. Parameters used in DWBA calculations.

Target	c (fm)	$(c_n - c_p)$ (fm)	a (fm)	V (MeV)	V_I (MeV)	R_I (fm)	A_I (fm)
^{90}Zr	4.90[b]	0.18	0.515[b]	40.2	40.9	4.77	1.242
^{116}Sn	5.43[a]	0.18[a]	0.515[a]	36.7	23.9	6.45	1.047
^{208}Pb	6.67[b]	0.26[a]	0.545[b]	43.3	61.4	7.75	0.567

[a]Reference [13].
[b]Reference [19].

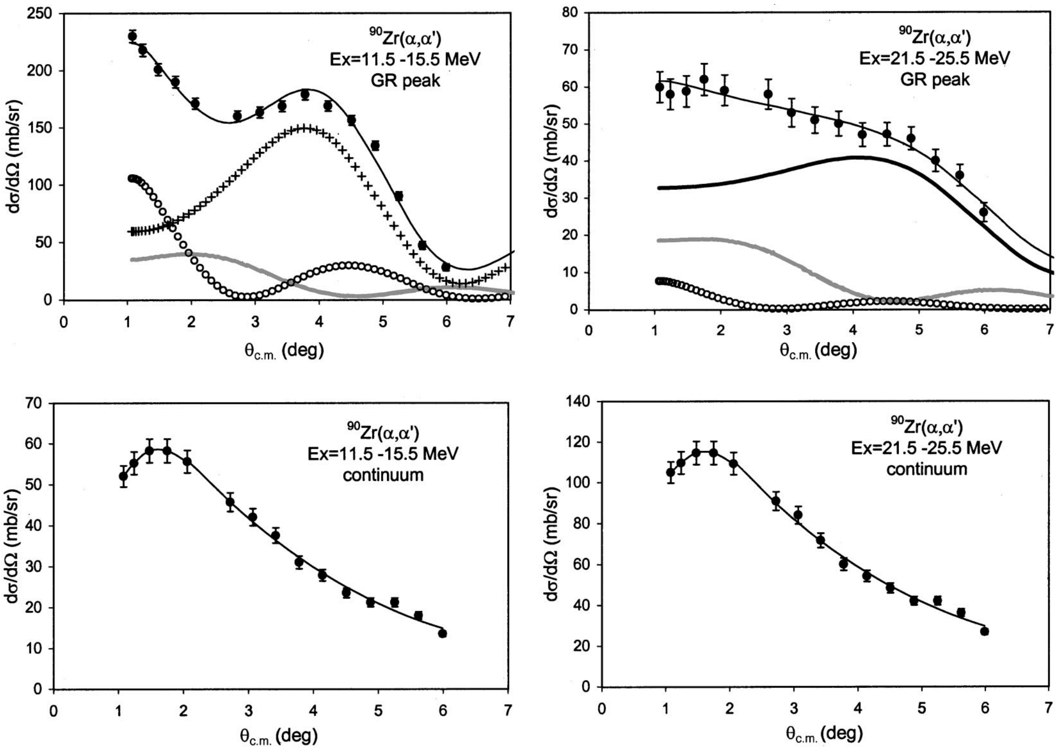

FIG. 2. Angular distributions of the differential cross section for inelastic α scattering for two excitation ranges of the GR peak and the continuum in ^{90}Zr plotted vs the average center-of-mass angle. The solid lines show the sum of the distributions for the individual multipolarities for the GR peak. The open circles show the $L=0$ component, the crosses show the $L=2$ component, the wide gray line shows the $L=1$ $T=0$ component, and the wide black line shows the $L=3$ component for each of the regions. When not shown, errors are smaller than the data points. The solid lines on the continuum distributions indicate the distribution trend.

excited in α scattering both by Coulomb excitation and by the nuclear force due to differences in neutron and proton distributions in the target nucleus. The nuclear transition density for the IVGDR is given by [13]

$$g_1(r)=\alpha_1\gamma((N-Z)/A)[d/dr+(1/3)cd^2/dr^2]\rho(r),$$

where $\alpha_1{}^2=\pi\hbar^2A/2mNZE_x$, $\gamma=3(c_n-c_p)A/(2c(N-Z))$ and c, c_n, and c_p are the respective matter, neutron, and proton radii. The transition densities and sum rules for the other multipolarities are described by Satchler [13] and the versions used in this work are given in Ref. [9]. Density dependent single folding calculations as described in Ref. [11] and by Satchler and Khoa [14] were carried out with optical model parameters obtained from elastic scattering [15,16] for each of the nuclei studied. Such calculations have been shown [11,14,15] to give cross sections that fit the data for low-lying states when using $B(EL)$ values from electromagnetic measurements. The calculations were carried out with the code PTOLEMY [17]. Input parameters for PTOLEMY were modified [18] to obtain a relativistic kinematically correct calculation. Radial moments were obtained by numerical integration of the Fermi mass distributions for each nucleus. The folding model and Fermi parameters as well as c_n-c_p values used in this work are given in Table I.

The multipole components of the giant resonance peak were obtained by dividing the spectra into a peak and continuum (indicated by the solid lines in Fig. 1), then dividing the peak into multiple regions (bins) by excitation energy. The angular distributions obtained for each of these bins was then compared to distorted wave Born approximation (DWBA) calculations to obtain the multipole components [11]. This technique is described in Ref. [11] for ^{24}Mg where isoscalar $E0$, $E1$, $E2$, and $E3$ strength distributions were

TABLE II. Parameters obtained for upper and lower components of the ISGDR.

	Lower			Upper		
A	Centroid (MeV)	rms width (MeV)	Strength %$E1$ EWSR	Centroid (MeV)	rms width (MeV)	Strength %$E1$ EWSR
^{208}Pb	12.2 ± 0.6	1.9 ± 0.5	32 ± 12	19.9 ± 0.8	2.5 ± 0.6	115 ± 20
^{116}Sn	14.7 ± 0.5	1.6 ± 0.5	38 ± 12	23.0 ± 0.6	3.7 ± 0.5	100 ± 15
^{90}Zr	16.2 ± 0.8	1.9 ± 0.7	19 ± 6	25.7 ± 0.7	3.5 ± 0.6	103 ± 18

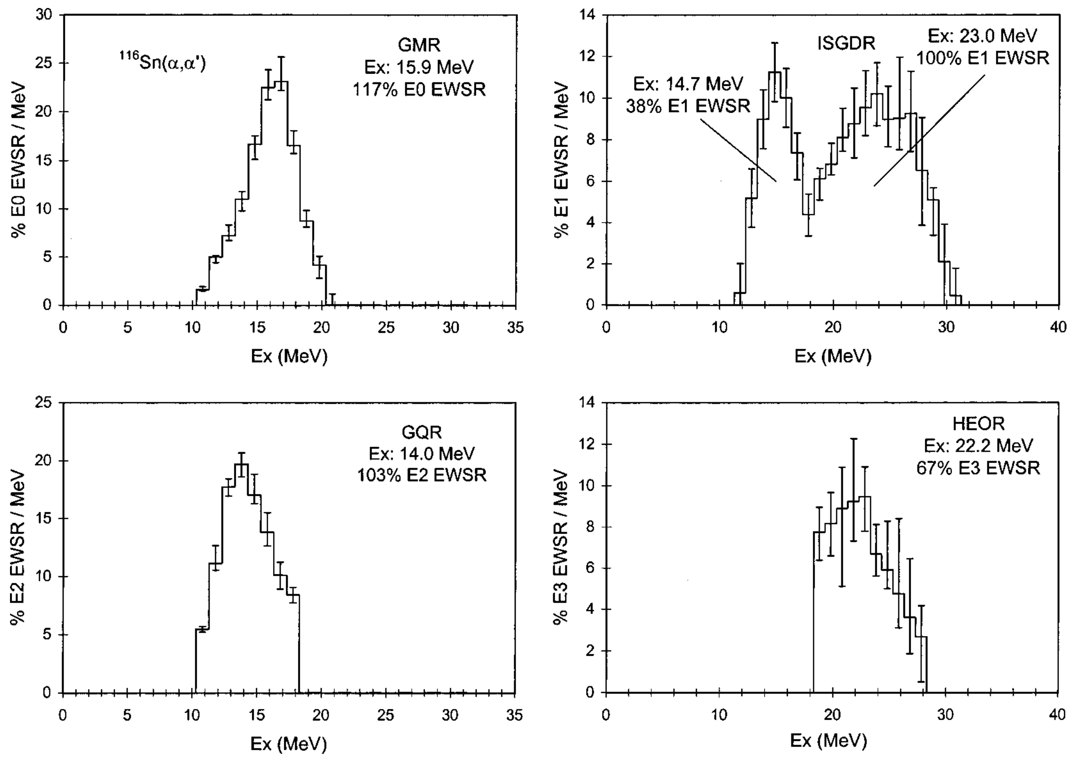

FIG. 3. The percentages of the isoscalar $E0$, $E1$, $E2$, and $E3$ EWSR/MeV obtained for ^{116}Sn are shown by the histograms. The error bars represent the uncertainty due to the fitting of the angular distributions as described in the text.

extracted up to $E_x \sim 40$ MeV. A sample of the angular distributions obtained for the giant resonance (GR) peak and the assumed continuum in ^{90}Zr are shown in Fig. 2. Fits to the angular distributions were carried out with a sum of isoscalar 0^+, 1^-, 2^+, 3^-, and 4^+ strengths. The isovector giant dipole resonance (IVGDR) contributions were calculated from the known distributions [20] and held fixed in the fits. Sample fits obtained, along with the individual components of the fits, are shown superimposed on the data in Fig. 2.

The ''continua'' illustrated by the lines in Fig. 1 were obtained by matching the slope and strength of the continuum above the GR peak, and decreasing this smoothly to 0 near the particle threshold, then adding in the known low energy octupole resonance (LEOR). The effects of the continuum choice were explored by also carrying out analyses using two other continua, one higher and one lower, each at the limits of plausibility. Because of discrete states, the LEOR, and the detector threshold, the continuum is most poorly defined at low excitation and these other continua differed the least at the highest excitation.

In the ^{24}Mg analysis [11] it was demonstrated that $E0$ strength in the peak and continuum could be identified, and that the total $E0$ strength obtained is essentially independent of continuum choice. That was also found to be true in these nuclei. However in the ^{24}Mg analysis [11] it was also demonstrated that other processes in the continuum gave angular distributions that could be fit with a sum of $E1$, $E2$, $E3$, and $E4$ multipole strengths and hence strength distributions for these multipoles could be very sensitive to assumptions about the continuum. In the present analyses, the $E1$ distributions were relatively insensitive to the different continua used, with the strength changing about 30% from the highest to lowest continuum because the continuum at high excitation is well defined. The $E2$ and $E3$ strengths were very sensitive to the continuum assumptions, and with the highest continuum chosen each decreased to less than half the expected strength. The centroids of all the distributions differed little with the different continuum assumptions, but the widths of the $E2$ and $E3$ distributions changed by up to about 20%.

TABLE III. Comparison of centroids to Colo *et al.* [22] calculations.

	Lower component			Upper component		
A	Exp. (MeV)	Colo *et al.* (MeV)	Difference (MeV)	Exp. (MeV)	Colo *et al.* (MeV)	Difference (MeV)
^{208}Pb	12.2	10.9	1.3	19.9	23.9	−4.0
^{116}Sn	14.7	12.5	2.2	23.0	27.5	−4.5
^{90}Zr	16.2	14.5	1.7	25.7	30.0	−4.3

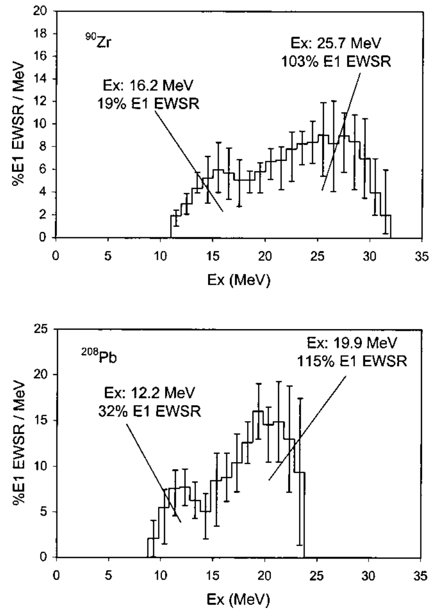

FIG. 4. Percentages of the isoscalar $E1$ EWSR/MeV obtained for ^{90}Zr and Pb are shown by the histograms. The error bars represent the uncertainty due to the fitting of the angular distributions as described in the text.

The multipole distributions obtained for ^{116}Sn are shown in Fig. 3. For each nucleus, the $E0$ distributions obtained are very similar to those reported in Ref. [12], which were obtained with a deformed potential analysis while the $E2$ distributions agreed with those in the literature. The $E3$ distributions obtained contained approximately 2/3 of the $E3$ EWSR as expected, with the remainder in the $1\hbar\omega$ excitations.

The $E1$ strength distribution in each nucleus (shown in Fig. 3 for ^{116}Sn and Fig. 4 for ^{90}Zr and ^{208}Pb) consists of two components, a broad component at $E_x \sim 114/A^{1/3}$ MeV containing approximately 100% of the $E1$ EWSR and a narrower one at $E_x \sim 72/A^{1/3}$ MeV containing 19–38 % of the $E1$ EWSR. The energies and widths for the components were obtained by fitting a Gaussian to the lower peak in each spectrum then subtracting that Gaussian and obtaining the centroid and root-mean-square (rms) width for the remaining strength. The parameters obtained for the two components are summarized in Table II. The errors include the uncertainties of the fits and the continuum choices. For ^{208}Pb, the centroid and width (FWHM) obtained for the upper component (19.9 ± 0.8 MeV, 5.9 ± 1.4 MeV) are in agreement with the values from Morsch *et al.* [1] (21.3 ± 0.8 MeV, 5.9 ± 0.8 MeV) but not with those from Davis *et al.* [4] (22.4 ± 0.5 MeV, 3.0 ± 0.5 MeV). Because the cross section of the high energy octupole resonance (HEOR) is increasing toward larger angles, the substraction technique used by Davis *et al.* [4] should result in an over subtraction in the region of the HEOR, obscuring some of the lower excitation part of the ISGDR, qualitatively consistent with what is observed.

The lower component contains 15–28 % of the total ISGDR strength and is near the IVGDR, which was included in the analysis at the known strength. In order to account for the strength of the low energy component of the ISGDR in ^{116}Sn (as the IVGDR), $c_n - c_p$ would have to be increased a factor of 5 to 0.95 fm from the expected 0.18 fm [13]. A similar increase would be required for the other nuclei.

Recent calculations of the $r^3 Y_{10}$ response function by Kolomiets *et al.* [21] and Colo *et al.* [22] using HF-RPA with Skyrme interactions and by Vretenar *et al.* [23] using relativistic RPA show the ISGDR strength split into upper and lower components qualitatively similar to that observed here. The upper component in these calculations is the compression mode, whose energy depends on the compression modulus, while the energy of the lower component changes with mass but is essentially independent of compression modulus. Vretenar *et al.* [23] describe this lower mode as a ''kind of toroidal motion'' and a surface effect, not a volume compression effect. Colo *et al.* [22] did not report transition densities for the two modes, but Vretenar *et al.* [23] show that their transition density for this lower component is very different from the transition density for the higher mode.

There are substantial differences between theory and experiment for the energies of the two modes. The centroid energies for both modes are compared to the predicted values in Table III. The centroids of the higher (compression) mode calculated with interactions which reproduce GMR energies are about 4 MeV higher than the experimental centroids while the calculated centroids for the lower mode lie 1–2 MeV below the experimental values. Thus the experimental ''splitting'' of the ISGDR from the present data is 5–7 MeV less than that predicted in the calculations.

Poelhekken *et al.* [24], using small angle α scattering in coincidence with γ decay, identified isoscalar 1^- strength in ^{40}Ca, ^{58}Ni, ^{90}Zr, and ^{208}Pb, lying almost entirely below the $E_x = 10$ MeV threshold of the present experiment and below the strength predicted by Vretenar *et al.* and Colo *et al.* They identified 8% of the $E1$ EWSR in ^{90}Zr and 14.7% in ^{208}Pb. Because our effective solid angle changes rapidly below $E_x = 10$ MeV, we do not extract multipole strength there. However if we combine the 1^- strength identified by Poelhekken *et al.* [24] with the lower component we identify, the centroids for the lower strength in ^{90}Zr and ^{208}Pb are 14.4 MeV and 10.7 MeV, respectively, in agreement with the centroids calculated by Colo *et al.* (14.5 MeV, 10.9 MeV) and by Vretenar *et al.* (for ^{208}Pb only, 10.35 MeV). The combined strength in the lower peak is 24% and 42% for ^{90}Zr and ^{208}Pb, respectively, compared to 34% and 36% in the Colo *et al.* calculation. However, neither calculation shows strength at the energies where it is reported in Ref. [24].

In conclusion, an isoscalar dipole giant resonance has been identified in ^{90}Zr, ^{116}Sn, and ^{208}Pb having two components at approximately $E_x \sim 72/A^{1/3}$ MeV and $E_x \sim 114/A^{1/3}$ MeV. The higher component is identified as the compression mode predicted in RPA calculations, but lies about 4.5 MeV lower than expected. The lower component, containing 15–28 % of the total $E1$ strength, lies 1–2 MeV above a new surface mode resonance suggested in recent RPA calculation. If low-lying 1^- strength seen by Poelhekken *et al.* [24] in ^{90}Zr and ^{208}Pb is combined with our observed strength, then reasonable agreement is obtained with predicted centroids and fair agreement with predicted strengths for the lower components.

We wish to thank Shalom Shlomo for interesting discussions and also Umesh Garg, B. Kharraja, M. N. Harakeh, N. Kalantar-Nayestanaki for their participation in an experimental run. This work was supported in part by the U.S. Department of Energy under Grant No. DE-FG03-93ER40773 and by The Robert A. Welch Foundation.

[1] H. P. Morsch, M. Rogge, and C. Mayer-Boricke, Phys. Rev. Lett. **45**, 337 (1980).
[2] H. P. Morsch *et al.*, Phys. Rev. C **28**, 1947 (1983).
[3] G. S. Adams *et al.*, Phys. Rev. C **33**, 2054 (1986).
[4] B. A. Davis *et al.*, Phys. Rev. Lett. **79**, 609 (1997).
[5] T. J. Deal, Nucl. Phys. **A217**, 210 (1973).
[6] M. N. Harakeh and A. E. L. Dieperink, Phys. Rev. C **23**, 2329 (1981).
[7] S. Stringari, Phys. Lett. **108B**, 232 (1982).
[8] N. Van Giai and H. Sagawa, Nucl. Phys. **A371**, 1 (1981).
[9] D. H. Youngblood, Y.-W. Lui, and H. L. Clark, Phys. Rev. C **55**, 2811 (1997).
[10] D. H. Youngblood, H. L. Clark, and Y.-W. Lui, Phys. Rev. C **57**, 1134 (1998).
[11] D. H. Youngblood, Y.-W. Lui, and H. L. Clark, Phys. Rev. C **60**, 014304 (1999).
[12] D. H. Youngblood, H. L. Clark, and Y.-W. Lui, Phys. Rev. Lett. **82**, 691 (1999).
[13] G. R. Satchler, Nucl. Phys. **A472**, 215 (1987).
[14] G. R. Satchler and Dao T. Khoa, Phys. Rev. C **55**, 285 (1997).
[15] H. L. Clark, Y.-W. Lui, and D. H. Youngblood, Phys. Rev. C **57**, 2887 (1998).
[16] H. L. Clark, Y.-W. Lui, and D. H. Youngblood (unpublished).
[17] M. Rhoades-Brown, M. H. Macfarlane, and S. C. Pieper, Phys. Rev. C **21**, 2417 (1980); M. H. Macfarlane and S. C. Pieper, Argonne National Laboratory Report No. ANL-76-11, Rev. 1, 1978 (unpublished).
[18] G. R. Satchler, Nucl. Phys. **A540**, 533 (1992).
[19] G. R. Satchler, Nucl. Phys. **A579**, 241 (1994).
[20] S. S. Dietrich and B. L. Berman, At. Data Nucl. Data Tables **38**, 199 (1988).
[21] A. Kolomiets, O. Pochivalov, and S. Shlomo, Progress in Research 1998–1999, Cyclotron Institute, Texas A&M University (unpublished).
[22] G. Colo, N. Van Giai, P. F. Bortignon, and M. R. Quaglia, Phys. Lett. B **485**, 362 (2000).
[23] D. Vretenar, A. Wandelt, and P. Ring, Phys. Lett. B **487**, 334 (2000).
[24] T. D. Poelhekken, S. K. B. Hesmondhalgh, H. J. Hofmann, A. van der Woude, and M. N. Harakeh, Phys. Lett. B **278**, 423 (1992).